steel research international

From High-Entropy Alloys to High-Entropy Steels

Dierk Raabe,* Cemal Cem Tasan, Hauke Springer, and Michael Bausch

Inspired by high-entropy alloys, we study the design of steels that are based on high configurational entropy for stabilizing a single-phase solid solution matrix. The focus is placed on the system Fe–Mn–Al–Si–C but we also present trends in the alloy system Fe–Mn–Al–C. Unlike in conventional high-entropy alloys, where five or more equiatomically proportioned components are used, we exploit the flat configurational entropy plateau in transition metal mixtures, stabilizing solid solutions also for lean, non–equiatomic compositions. This renders the high-entropy alloying concept, where none of the elements prevails, into a class of Fe-based materials which we refer to as high-entropy steels. A point that has received little attention in high-entropy alloys is the use of interstitial elements. Here, we address the role of C in face-centered cubic solid solution phases. High-entropy steels reveal excellent mechanical properties, namely, very high ductility and toughness; excellent high rate and low-temperature ductility; high strength of up to 1 GPa; up to 17% reduced mass density; and very high strain hardening. The microstructure stability can be tuned by adjusting the stacking fault energy. This enables to exploit deformation effects such as the TRIP, TWIP, or precipitation determined mechanisms.

1. Introduction and Motivation

1.1. High-Entropy Alloys

Multi-component alloys[1–8] which are also referred to as high-entropy alloys[9–16] represent a class of metallic materials containing typically five or more principal alloying elements in equiatomic or near equiatomic proportions. While early efforts in this direction were inspired from recipe guidelines devised originally for metallic glasses, the current work in this field aims at designing crystalline entropy-stabilized massive solid solution phases of equiatomic composition. The concepts of designing such compositionally complex solid solutions were introduced and further developed by the groups of Cantor,[1–7] Ranganathan,[8] and Yeh.[9–16]

By building on solid solution principles that originate from some of the well-known Hume-Rothery rules,[17,18] a number of phenomenological alloying guidelines were suggested in this context, such as the condition that the absolute value of the mixing enthalpy should preferably be placed between $(-2.685\delta–2.54)$ kJ mol^{-1} $< H_{\mathrm{mix}} < (-1.28\delta + 5.44)$ kJ mol^{-1}, where δ is a constraining parameter describing upper bounds for the atomic size difference. Also, it was inferred that the mixing entropy should assume a value above 1.61 R with R being the gas constant. The empirically observed relevance of the valence electron concentration (VEC) for solid solutions has led to a corresponding design guideline, suggesting VEC $\leq$ 6.87 for stable body-centered cubic (bcc) and VEC $\geq$ 8 for stable face-centered cubic (fcc) phases.[19–23]

It should be considered in that context that different definitions for the valence electron concentration calculations exist in the literature. Sometimes also different valence numbers are used specifically for some of the transition metals with d electrons.[17,18,22–25]

As discussed in more detail below, many of the non-equiatomic Fe–Mn-based high-entropy steels presented in this paper have a VEC of 7–8 when only counting the substitutional elements (we use here the VEC definition given in the paper of Guo et al.[23]). However, when additionally counting the electrons provided by interstitial elements such as C and N, the high-entropy steels presented here reach VECs above 8.

This observation suggests that for synthesizing high-entropy alloys with a stable fcc matrix, alloying and the associated electron donation provided by interstitial elements could become an interesting new design variant.

1.2. Deviating from Equiatomic Composition: High-Entropy Steels

The original high-entropy or respectively multi-component alloy concepts outlined above serve as a starting point for designing compositionally complex yet non-equiatomically proportioned Fe-based materials.

[*] D. Raabe, C. C. Tasan, H. Springer, M. Bausch
Max-Planck-InstitutfürEisenforschung, Department for Microstructure Physics and Alloy Design, Max-Planck-Str. 1, 40237 Düsseldorf, Germany
Email: d.raabe@mpie.de

DOI: 10.1002/srin.201500133

The high-entropy design rules introduced above also apply to some extent here, however, we additionally consider interstitial alloying elements, specifically solute C. We emphasize the latter point since corresponding massive solid solution effects associated with interstitial elements have not yet been considered in multi-component transition metal alloys. Interstitial elements, specifically C and N, offer very interesting alloying options with respect to stabilizing fcc solid solutions as is also expressed by their effect on the VEC.

A second design idea, deviating from the classical multi-component concept, lies in using relatively lean and non-equiatomically portioned compositions.[26,27] This is due to the fact that in many transition metal alloy solid solutions, the shape of the configurational entropy as a function of chemical composition assumes a relatively flat and compositionally wide plateau. This means that the entropy curve has a weak maximum and no steep changes, except for the case of very small concentrations.[68]

This fact suggests that entropy-based stabilization of massive solid solutions can also be achieved for non-equiatomic quinary and quaternary alloy composi-tions.[26,27,68]

This modifies the original high entropy alloying concept, where none of the alloying elements were meant to dominate, into a class of Fe-based materials which we consequently refer here to as high-entropy steels.

Beyond the argument associated with the flat entropy curve, there are other good reasons for designing compositionally simplified high-entropy alloys:

An obvious motive lies in reducing alloying costs. Any material that is being designed and meant to be used for specific applications must pass the critical test whether the respective alloying elements and their quantities are indeed required to reach a certain design target or not. If not, their respective alloying content can be reduced. Examples are typical bounds known for established commercial alloys such as a certain Cr and Mo content in stainless steels for achieving sufficient pitting and corrosion resistance; specific values of Ni and Al in superalloys required to arrive at the characteristic matrix —precipitate structure; a certain Cu content for precipitating Guinier–Preston zones in age hardening aluminum alloys; or a minimum required Nb or Ta content to stabilize elastically compliant bcc Ti alloys.

In all these metallurgical examples, the respective alloying elements are only added to the content that is required for achieving the aims described, but the alloying content is not increased beyond these values if not serving a specific thermodynamic, kinetic, or property function. However, in cases where a near-maximum value of the configurational entropy can be realized at smaller alloying content, i.e., before reaching an equiatomic composition, no need exists to alloy further. In other words, the presence of a long and flat compositional entropy plateau enables to exploit a wider mixing range and less consumption of expensive alloying ingredients when designing high-entropy alloys.[26,27]

Another issue in realizing homogeneous massive crystalline solid solutions is not the maximization of the entropy but rather the avoidance of intermetallic phases.[26–29] When aiming at stabilizing a single-phase compositionally complex material, it is from a thermodynamic standpoint more plausible to analyze the likelihood of intermetallic compounds in the multi-component phase diagram rather than only analyzing the configurational entropy.

A good example for this rationale was recently documented in the works of Tasan et al.[27,68] The authors showed that the entropy-maximized 25% equiatomic quaternary FeMnCoCr alloy (being close to the well-known Cantor alloy) surprisingly leads to a complex multiphase microstructure containing several intermetallic phases while the non-equiatomic material Fe40Mn10Co10Cr produces a homogeneous fcc single phase. This shows that a high-entropy contribution to the stabilization of the matrix alone is often not sufficient to over-compensate enthalpy advantages of competing intermetallic phases. This might be also the reason why truly single-phase high-entropy phases have been realized only for a few compositions so far. Introducing a non-equiatomic mixing rule would provide a much larger compositional space for synthesizing high-entropy alloys without intermetallic phases.

A third set of advantages associated with lean multi-component compositions is a practical one, such as reducing variations in vapor pressure typically occurring in multi-component systems, less segregation, and improved casting properties.

Another aspect that should be realized is that XRD, EBSD, and atom probe tomography analysis increasingly reveals that many of the high-entropy alloys that have been studied so far are actually not single-phase materials but often contain intermetallic phases.[29–32]A well-investigated exception from this is the multi-component yet single-phase fcc Cantor alloy FeMnNiCoCr.[3,7,28,33,34]

The occurrence of one or often more intermetallic phases, sometimes with nanoscopic size or at grain boundaries,[29] is not only a thermodynamic or kinetic issue. The presence of intermetallic phases typically deteriorates mechanical key properties such as ductility, fatigue resistance, and toughness. Alloys containing intermetallic phases, therefore, often reveal inferior properties compared to corresponding single-phase alloys of similar, yet non-equiatomic composition.[68]

An additional point supporting non-equiatomic multi-component alloys in the form of high-entropy steels is to better exploit fcc phase stabilization and strain hardening effects associated with interstitial elements, specifically C which has been well studied in the context of TWIP steel systems.[35–55]

In the light of these considerations, we present a set of different multi-component high-entropy steels that make use of increased configurational entropy for stabilizing a single-phase homogeneous massive solid solution fcc matrix. The focus is placed on the quinary system Fe–Mn–Al–Si–C but also some trends in the quaternary

system Fe–Mn–Al–C are presented. Some of the alloys discussed contain as little as 50 at% Fe. High-entropy steels based on the quinary Fe–Mn–Al–Si–C system overlap for the case of a maximized Al content in part with the recently introduced class of low-density steels.[56–63] In these alloys, the size and high stability of the fcc phase field created by Fe, Mn, and C prevails even when adding a high amount of soluble Al. Increasing Al content enables density reduction and scalable precipitation strengthening as outlined in the ensuing section in more detail.[56–67]

The valence electron rule for realizing stable fcc solid solutions was in the high-entropy alloy literature suggested as VEC $\geq$ 8.[19–23]

When calculating the VEC for the fcc high-entropy steels presented here, including also compositions presented in some of our earlier publications,[62,63,67] we find typical values for the VEC of 8–9. The VEC numbers for the individual elemental are 3 for Al, 8 for Fe, 7 for Mn, 4 for Si, 4 for C, and 5 for N.[23]

It is interesting to note that we find smaller VEC numbers (typically 7–8) for our current non-equiatomic Fe–Mn-based high-entropy steels when considering only the substitutional elements Fe, Mn, Al, and Si and neglecting the VEC contribution provided by the interstitial elements. When also considering the additional electrons donated by interstitials, for instance by the very high-C content, the alloys reach VECs above 8.This means that the VEC criterion suggests that fcc solid solution high-entropy steels can be designed when using interstitial elements. This pathway opens a further alloy design option for high-entropy alloys.

Another important aspect in that context is to define the fcc phase stability that is actually targeted. From the experience with highly alloyed fcc steels,[42–56] it is well known that typically not the stable fcc matrix but rather a slightly instable fcc matrix provides beneficial strain hardening properties. More specific, when aiming at fcc solid solutions where coupled deformation–transformation effects such as TRIP and TWIP are to be exploited as mechanisms for equipping these alloys with additional strain hardening capacity, the target is actually not to achieve a thermodynamically stable but rather an instable matrix. This enables deformation-induced-confined phase transformations such as martensite or twinning. This has been recently also demonstrated for the case of high-entropy alloys.[68]

This means that, when translating this idea back into the VEC guideline, it might be a design criterion to target a VEC value of just 8 but not much higher.

One has to consider though that the current high-entropy alloy literature suggests that the VEC criterion alone is an insufficient design criterion. Instead, reliable phase predictions require full thermodynamic calculations whenever possible.

2. Synthesis, Processing, and Characterization

More than 25 different high-entropy steels with different compositions based on the quinary system Fe–Mn–Al–Si–C were synthesized and probed over the last years particularly by the group of Frommeyer,[56–73] **Table 1**. Corresponding isothermal sections of both, the Fe–Mn–Al and the Fe–Mn–Si systems, which are similar for small Al and Si alloying, were discussed before in the literature.[56–61,68–73]

A subsection through the quaternary Fe–Mn–Al–C phase diagram at Fe–26 wt% Mn, using data from,[56–73] is shown in **Figure 1**a.

Weight [%]					Atomic [%]				
Mn	**Al**	**Si**	**C**	**Fe**	**Mn**	**Al**	**Si**	**C**	**Fe**
20	2.7	2.7	0.15	74.45	19.10	5.25	5.04	0.66	69.95
18	2.7	2.7	0.30	76.30	17.11	5.23	5.02	1.30	71.34
20	2.7	2.7	0.50	74.10	18.87	5.19	4.98	2.16	68.79
25	2.7	2.7	0.05	69.55	23.94	5.26	5.06	0.22	65.52
20	0.0	0.0	1.2	78.80	19.42	0.0	0.0	5.33	75.26
20	2.0	0.0	1.2	76.80	19.03	3.87	0.0	5.22	71.88
20	5.0	0.0	1.2	73.80	18.47	9.40	0.0	5.07	67.06
20	8.0	0.0	1.2	70.80	17.95	14.62	0.0	4.93	62.51
20	11.0	0.0	1.2	67.80	17.45	19.55	0.0	4.79	58.21
24	22.5	0.0	1.0	52.50	19.04	36.35	0.0	3.63	40.98

Table 1. Table showing weight percent (wt%) and atomic percent (at%) for some of the important high-entropy steels studied in this paper.

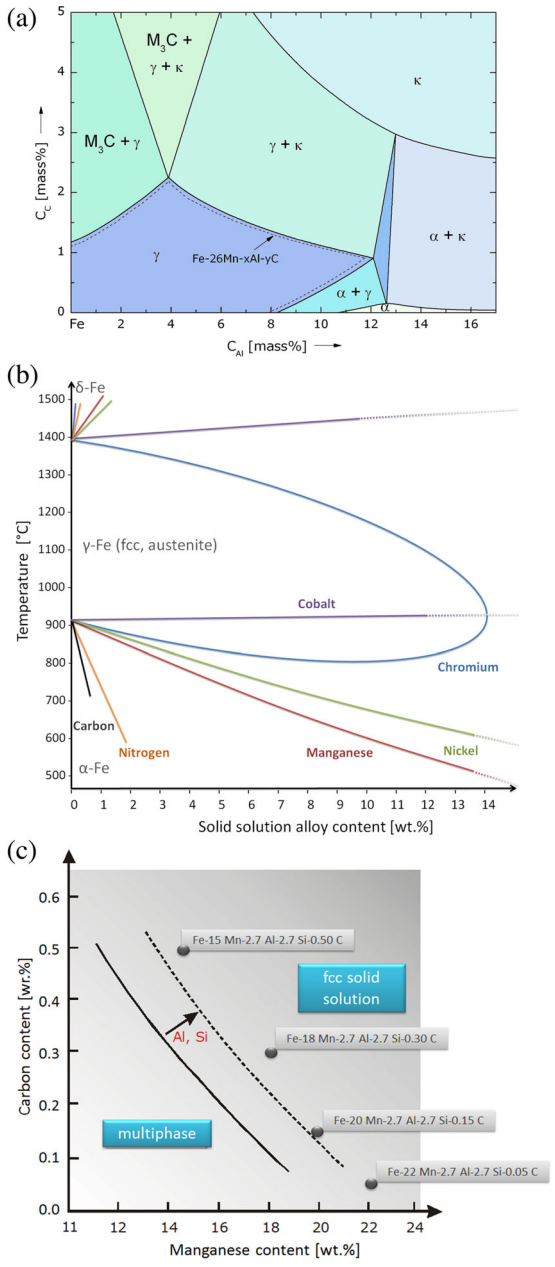

Figure 1. a) Isothermal section (900 °C) taken through the quaternary Fe–Mn–Al–C phase diagram reproduced using published data and phase observations from several groups.[56–73] b) Binary effects of various solid solution alloying elements in a Fe matrix which are suited as matrix components for stabilizing high-entropy steels with a single face-centered cubic matrix (austenite). Particularly, the elements C, N, Mn, and Ni expand the phase field of the austenite also down to room temperature and even to cryogenic application regimes. For less than 10 wt% percent also Cr, which is sometimes regarded as a ferrite stabilizing element, increases the austenitic phase field. c) C and Mn alloying effects on the fcc solid solution stability for quinary FeMnAlSiC systems including schematically also the influence of Al and Si which reduce the austenitic phase field. The diagram shows some of the alloys tested in this work. They have different VECs and different stability of the fcc phase when mechanically loaded. Some of the alloys can undergo athermal deformation-stimulated martensite and twin transformation.

Elements such as Mn and Ni enhance the fcc γ-phase field in the Fe-rich corner of the phase diagram, Figure 1b. The strong stabilization of the γ-phase field is even further enhanced by the presence of interstitial solute C, Figure 1b, c. Thus, alloys containing high fractions of Mn (20–30 wt%) and C (0.5–1.5 wt%) reveal compositionally large and very stable fcc solid solution phase fields, Figure 1c.

Under such circumstances, substantial amounts of Al of up to 22 wt % (36 at%) can be additionally rendered into the same solid solution without opening a second phase field.[57] For instance in the Fe–Mn–Al ternary corner of the quaternary Fe–Mn–Al–C diagram, i.e., even without the presence of C, solid Fe–Mn solutions with 25–28 wt% Mn are austenitic at 1000 °C solving up to 6 wt% Al. In the same ternary corner of the phase diagram, the maximum solid solution content of Al is limited to about 9 wt% when the Mn concentration is increased to 40 wt%.

When solute interstitial C is additionally added, the fcc γ-phase field can be substantially broadened, as revealed by Figure 1c and by the isothermal Fe–30Mn–Al–C section, taken at 900 °C, from the quaternary phase diagram,[70–73] Figure 1a. The section shows a slightly contracted γ-phase field line for 26 wt% Mn. The neighboring phase fields, i.e., α + γ, γ + cementite, γ + κ-carbide, and α + γ are shifted accordingly. Further details are given in Ref. [72].

The alloys were synthesized via melting and casting in a vacuum induction melting furnace and cast under 400–900 mbar argon atmosphere into rectangular molds of $30 \times 60 \times 180$ mm^3 or $10 \times 50 \times 130$ mm^3 size, respectively. The cast blocks were then hot rolled at 1100 °C to thickness reductions between 80 and 90% and subsequently recrystallized and solution annealed at temperatures between 1075 and 1100 °C for 30 min, followed either by slow cooling in air or in some cases water quenching to room temperature.

Microstructure characterization was conducted by light optical microscopy, electron backscatter diffraction (EBSD) in conjunction with scanning electron microscopy (SEM), transmission electron microscopy (TEM), and x-ray diffraction (XRD). In some cases, atom probe tomography was conducted specifically when studying details associated with grain boundary segregation or the possible formation of second phases.[67,74]

Mechanical characterization was done by hardness testing and tensile testing in a temperature range between −50 and 400 °C and at initial strain rates of 10^{-3} s^{-1} up to 10^3 s^{-1} where the high deformation rates were realized by using split-Hopkinson tests.

3. Mechanical Properties and Deformation Mechanisms

Figure 2 shows the tensile test results for some of the quinary high-entropy steels for different deformation temperatures in the range between −50 and 300 °C. Some of these data were reproduced form earlier experiments

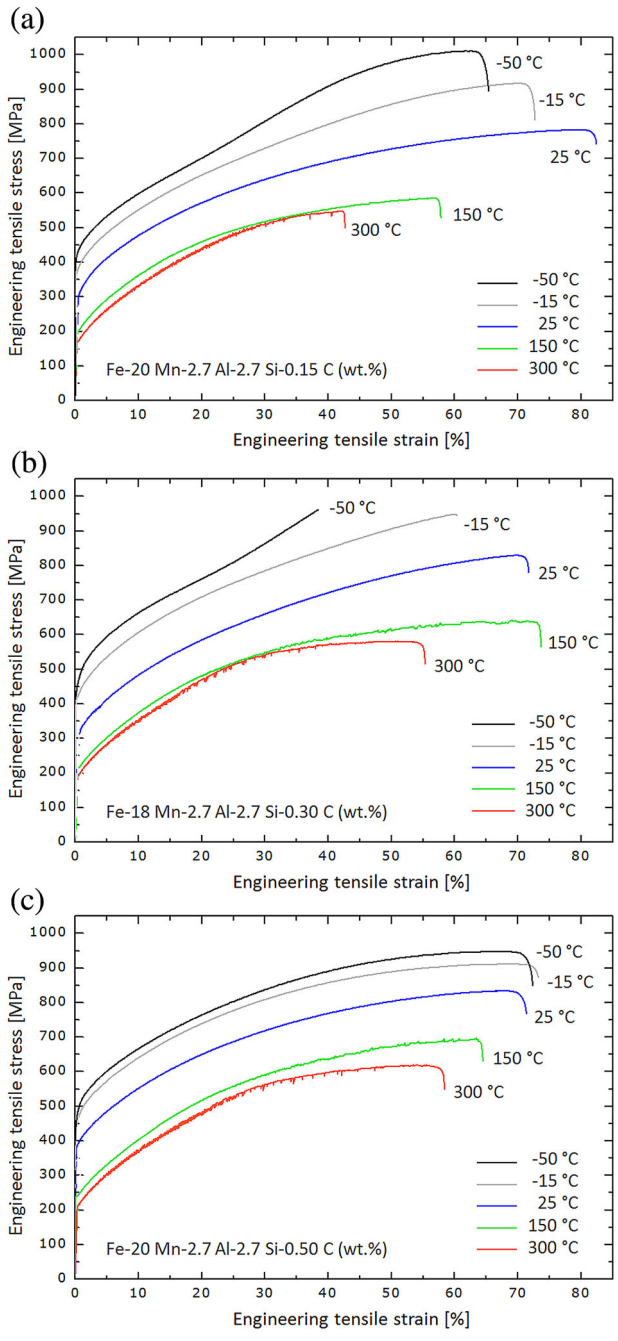

Figure 2. Stress–strain curves taken for quasi-static tensile tests conducted at different testing temperatures between −50 and 300 °C for high-entropy steels in the quinary system Fe–Mn–Al–Si–C. The trend toward deformation-induced martensite formation, resulting from different degrees in stability of the fcc solid solution phase at the onset of plastic straining, leads to different strain hardening characteristics (see also martensite characterization shown in Figure 3). Some of the curves are reproduced from earlier experiments conducted by the group of Frommeyer.[56–61,73,75] Of special relevance is the high ductility and high ultimate tensile strength observed at cryogenic temperatures of −50 °C. a) Fe–20Mn–2.7Al–2.7 Si–0.15 C (wt %); b) Fe–18 Mn–2.7 Al–2.7 Si–0.30 C (wt%); c) Fe–20 Mn–2.7 Al–2.7 Si–0.50 C (wt%). The experimental scatter was 1–4% for the ultimate tensile strength and 2–5% for the tensile elongation. The scatter was larger at higher temperatures.

conducted by the group of Frommeyer.[74] The experimental scatter for the tensile tests was 1–4% for the ultimate tensile strength and 2–5% for the tensile elongation. The scatter was larger at higher temperatures.

Figure 2a shows excellent mechanical properties for an alloy containing 20 Mn, 2.7 Al, 2.7 Si, and 0.15C (wt%). The room temperature ductility is very high, exceeding 80% engineering tensile elongation. What is even more interesting is the excellent ductility also at low testing temperatures such as at −15 and −50 °C. At these cryogenic conditions, the material still reaches 60–70% elongation, respectively, at an even strongly increased flow stress. The sample tested at −50 °C reaches a tensile strength of 1 GPa. **Figure 3** reveals the corresponding volume fractions of martensite after deformation (taken at elongation to fracture). These data suggest that this enormous increase in strength at cryogenic conditions can be essentially attributed to the formation of martensite

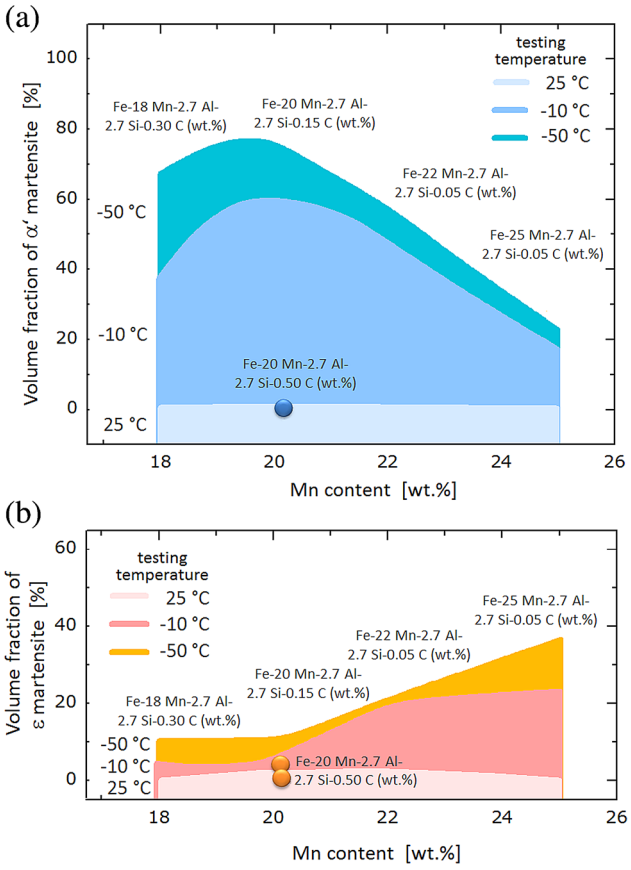

Figure 3. Martensite volume fraction observed at the end of tensile deformation for different types of high-entropy steels for three different temperatures, namely, 25, −10, and −50 °C. At the onset of plastic deformation, all materials are characterized by a massive solid solution fcc single-phase microstructure, i.e., the martensite is formed during tensile testing, explaining the observed strain hardening curves. a) α' martensite; b) ε-martensite. Some of the data are reproduced from experiments conducted by the group of Frommeyer.[56–61,73,75]

which is approaching 80% for this material at the fracture point. This very high volume fraction of deformation-induced martensite explains the excellent ductility and strength at the low testing temperatures. Also, the slightly concave shape of the stress–strain curve observed in Figure 2a indicates that at −50 °C very pronounced formation of martensite commences between 20 and 30% engineering strain. This mechanism leads to an additional contribution to the total strain hardening at this stage, explaining the very high ultimate tensile strength observed for this material.

Very similar stress–strain results, however, with ductility values typically not exceeding 50–55%, are also observed for conventional austenitic stainless steels such as the standard grade 304 (1.4301) which contains about 18 wt% Cr and 8 wt% Ni[76–81] and for certain duplex stainless steels with instable austenite.[82,83] These materials also show a similar increase in the flow stress when deformed at temperatures below room temperature, also due to deformation-induced martensite. However, they show much smaller values in the elongation to fracture compared to the current alloys.

Figure 2b shows the mechanical results at different temperatures for a material containing a similar Mn content but higher C content than the materials shown in Figure 2a. The alloy contains 18 Mn, 2.7 Al, 2.7 Si, and 0.30C (wt%). The alloy reveals rather similar features as the material shown in Figure 2a, however, the overall ductility observed at room temperature and at the low temperature regime is slightly smaller compared to the material with smaller C content, Figure 2a. At 150 and 300 °C, the alloy shows a slightly serrated flow behavior which is attributed to the effect of the solid C content on the mobile dislocations.

The stress–strain results for a related alloy with 0.5 wt% C, Figure 2c, shows in principle similar trends (20 Mn, 2.7 Al, 2.7 Si, 0.50C (wt%)). The ultimate tensile strength at cryogenic testing (−50 °C) is slightly below the one observed for the material with very low-C content (0.15 wt% C), Figure 2a. Microstructure analysis revealed that this high C containing alloy variant produces a much smaller volume fraction of deformation-stimulated martensite, as shown in Figure 3. This is attributed to the C-related high stability of the fcc phase field, as discussed above, Figure 1c.

The stress–strain data obtained from quasi-static tensile testing at room temperature shown in **Figure 4** reveals effects that are associated with the change in the Al content. As discussed above in terms of the section through the corresponding quaternary phase diagram (Figure 1), for the case of a relatively low-Mn content (here: 20wt%), an increased Al content may lead to the formation of secondary phases, irrespective of the very high-C content in the current alloy. Hence, materials were quenched after casting prior to testing. The possibility of the occurrence of a secondary phase is also suggested by some of the mechanical test data: the increase in the Al

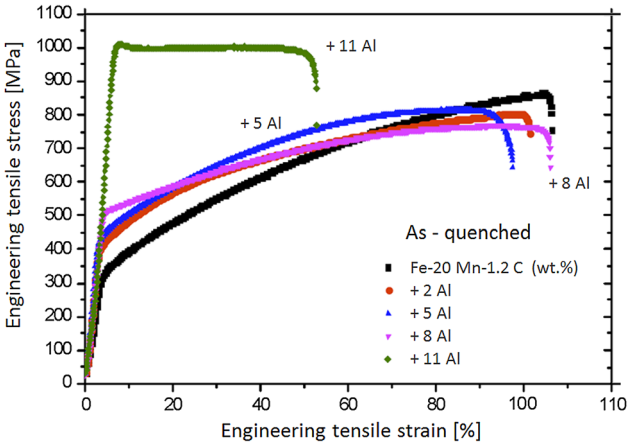

Figure 4. Stress–strain curves obtained from quasi-static tensile testing with an initial strain rate of 5 K s^{-1} at room temperature for a high-entropy steel with composition Fe–20Mn–1.2 C (wt%) and various amounts of Al ranging from 0% up to 11% (wt%). The scatter amounted to 1–4% for the ultimate tensile strength and 2–8% for the tensile elongation.

content between 0 and 8 wt% leads primarily to an increase of the solid solution strengthening. This can be inferred from the increase in yield strength from about 300 MPa up to about 500 MPa. This observation suggests that the material is in a single-phase solid solution state. The strain hardening is also quite similar among these variants.

One of the most remarkable mechanical property features of these high-entropy steels between 0 and 8 wt% Al is the very high elongation to fracture exceeding in part 100%. One should add, however, that the mechanical data shown in Figure 4 have been obtained by a high-throughput rapid alloy prototyping method using a smaller tensile gauge length[63] and need to be confirmed by norm-sized standard tensile tests. In any case, for room temperature deformation, i.e., low homologous temperatures, this is an extremely high value compared to most other alloy systems known to date.

One of the alloys has a remarkably different behavior, namely, the one with 11 wt% Al, Figure 4. The very high yield strength of about 1000 MPa and specifically the nearly horizontal shape of the stress–strain curve are a very interesting and quite unexpected feature of this alloy. We suggest that in the as-quenched state the alloy with 11 wt% Al, as probed here, is no longer in the state of an fcc solid solution. What is particularly remarkable about this high Al-containing specimen is the horizontal flow curve. Although the material does practically not reveal any strain hardening but instead even a minor stress drop at the beginning of yielding, the material does not seem to become instable but can rather be deformed to about 50% elongation prior to fracture. This is a very unusual behavior. Typically, metallic alloys which do not undergo any substantial strain hardening do not reach such a huge ductility at these high strength levels. The underlying microstructural reason for this behavior is still subject to

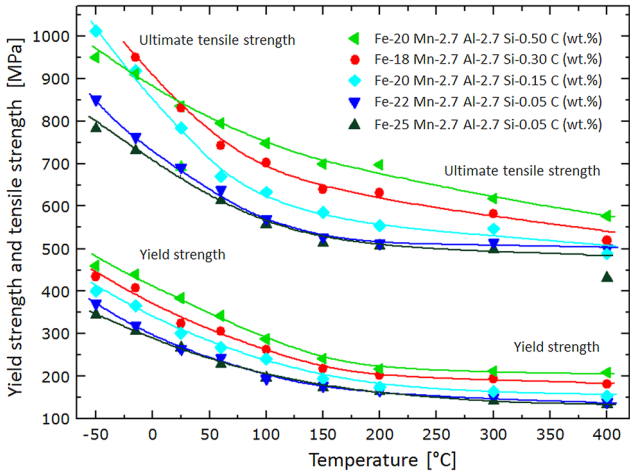

Figure 5. Overview of the stress–strain results in terms of the yield strength and the ultimate tensile strength obtained from quasi-static tensile testing at different temperatures for a group of different high-entropy steels in the quinary system Fe–Mn–Al–Si–C.[56–61,73,75] The scatter was 2–4% for the yield strength and 1–5% for the tensile strength. Testing at higher temperatures produced slightly larger scatter.

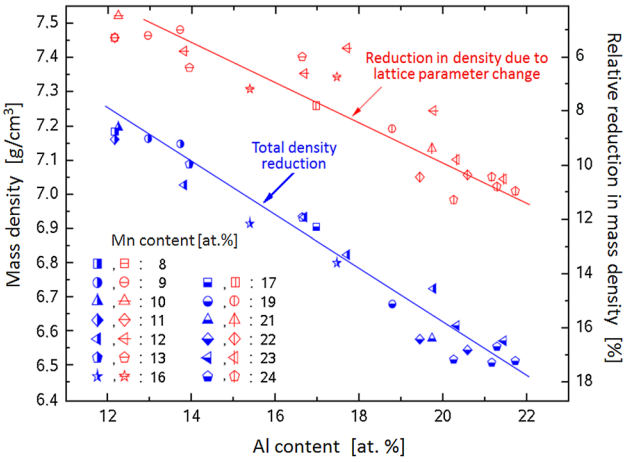

Figure 7. Compilation of the achievable reduction in the mass density for Al containing high-entropy steels according to data of Brüx.[73] The results are taken from earlier experiments conducted by the group of Frommeyer and Brüx.[56–61,73,75] The alloys have different C content.

further analysis but it might be due the presence of nanosized quenched-in κ-carbide precipitates.

Figure 5 shows for a set of quinary alloys the ultimate tensile strength and the yield strength data as a function of temperature. It can be nicely seen in this compilation that both, the yield strength and the tensile strength values drastically increase as the temperature is reduced. This means that this group of alloys has excellent cryogenic mechanical properties.

Figure 6 shows for the same alloys the evolution of the elongation to fracture observed in tensile tests as a function of temperature. It is observed that the ductility increases drastically as the temperature is reduced for most of the alloys.

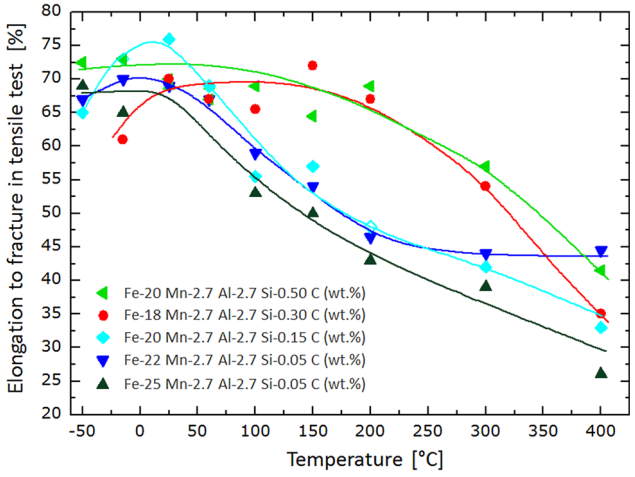

Figure 6. Overview of the results obtained for the elongation to fracture measured in the quasi-static tensile tests at different temperatures for a group of different high-entropy steels in the quinary system Fe–Mn–Al–Si–C.[56–61,73,75] The scatter for the elongation was 2–8%.

Besides their excellent low-temperature properties, high-entropy steels also provide another very important advantage compared to other massive solid solution alloys, specifically when alloyed with very high-Al content: **Figure 7** shows the reduction in mass density that is associated with an increase in Al content in solid solution. Two effects are highlighted: the first one is the reduction in mass density that is related to the change in the fcc lattice parameter due to the massive solid solution achieved in these high-entropy alloys. The second effect is simply due to the low molar weight of the Al atoms. Both effects together lead to a total reduction in the mass density of such alloys of up to 17% compared to the mass density of Fe. This is an enormous advantage in fields where mass reduction is a crucial point such as in automotive and aerospace applications but also for cranes or complex and mechanically highly loaded constructions. It should be noted though that solute Al also reduces the elastic modulus of high-entropy steels and not only their mass density.[56–63]

When comparing the alloy concept and some properties of the non-equiatomic high-entropy steels presented here with those of conventional equiatomic high-entropy alloys, a number of similarities but also some differences become apparent as summarized in **Table 2**. When compared to the properties of conventional high-entropy alloys and even to those of other classes of steels, the mechanical properties of high-entropy steels offer interesting opportunities for designing future light weight, highly ductile, and high-strength alloys. **Figure 8** presents a compilation of some typical ranges for the total elongation to fracture and the ultimate tensile strength

Property	Non-equiatomic high-entropy steels	Equiatomic high-entropy alloys
Single-phase solid solution	Easier to realize single-phase states, since the equiatomic mixing rule is relaxed and intermetallic phases can be better avoided; some thermodynamic data for several Fe-based ternary and some quaternary alloys are available	Realized only for few alloys so far since equiatomic mixing rule leaves little room for compositional variation to avoid intermetallic phases; high matrix entropy alone is often not sufficient to over-compensate the enthalpy of competing intermetallic phases
Design of phase stability	Easier to realize since equiatomic mixing rule is relaxed and wide choice of compositional variations enables to tune the stacking fault energy; can be used to enable TWIP and TRIP effects	Phase stability can only be designed by picking other equiatomic elemental combinations
Interstitials	Use of interstitial elements such as C, N, and probably B contributes further degrees of freedom for designing alloys with high fcc phase stability and for tuning desired stacking fault energy levels; opportunity of introducing TWIP and TRIP effects	Interstitials not used so far
High-temperature stability	Good high-temperature stability; wider compositional variations allow to design and tune precipitations	Good high-temperature stability
Alloy costs	Relaxing equiatomic mixing rule enables to better avoid use of expensive and unnecessary alloying elements	Equiatomic mixing rule makes it difficult to avoid expensive alloying elements
Solid solution strengthening	Solid solution strengthening confined to non-equiatomic proportions	Maximum solid solution strengthening
Cryogenic properties	Excellent cryogenic mechanical properties	Excellent cryogenic mechanical properties
Toughness and ductility	Excellent toughness and ductility in part exceeding 100% under tensile load	Excellent toughness and ductility when alloy is in single-phase state such as the Cantor alloy; brittle when intermetallic phases are formed
Strain hardening	Can be compositionally fine-tuned to enable deformation-induced athermal deformation mechanisms such as twinning and martensite formation, i.e., TWIP and TRIP effects	Conventional strain hardening potential of fcc solid solution materials; maximum solution creates wide dislocation cores, reduced cross-slip and promotes low stacking fault energy
Strength	Very high and tunable strength	Excellent strength when alloy is in single-phase state such as the Cantor alloy; brittle when intermetallic phases are formed

Table 2. Similarities and differences between non-equiatomic high-entropy steels and equiatomic high-entropy alloys.

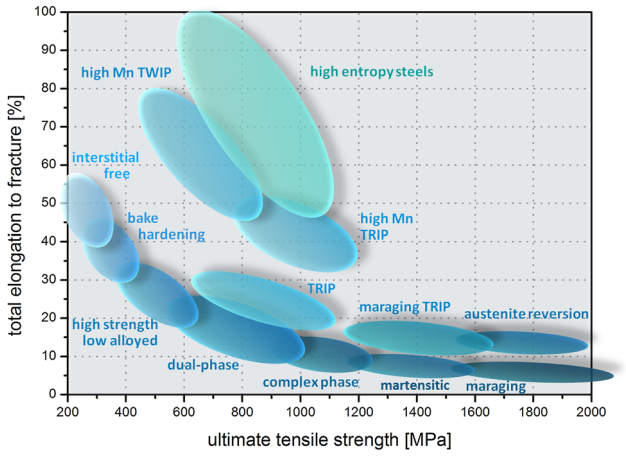

Figure 8. Overview diagram showing some typical value ranges for the total elongation to fracture and the ultimate engineering tensile strength for a number of different classes of steels. Additionally, the diagram includes data for high-entropy steels with quaternary FeMnAlC and quinary FeMnAlSiC composition, which in part exceed the mechanical properties known from many other types of alloys. The diagram reveals that the high-entropy steels are capable of covering a wide range of mechanical properties which is enabled by composition- and temperature-dependent tuning of phase stability for activating TRIP, TWIP, and precipitation effects. The properties of the TWIP and TRIP reference alloys are taken from Refs. [37–67]. They have compositions with up to 22 wt% Mn and 0.6 wt% C. The data for the dual phase reference steels are taken from Refs. [84–92] and for the maraging and austenite reversion steels from Refs. [93–99].

for different classes of steels. The diagram also includes data for high-entropy steels with quaternary FeMnAlC and quinary FeMnAlSiC composition, which in part exceed the mechanical properties known from many other types of alloys. The diagram reveals that the high-entropy steels are capable of covering a very wide range of mechanical properties which is enabled by composition- and temperature-dependent tuning of phase stability for TRIP, TWIP, and precipitation effects. In many cases, even a single quinary FeMnAlSiC high-entropy steel composition can match, through adequate heat treatments, a wide range of requested mechanical properties.

4. Conclusions and Outlook

In this paper, we presented a number of surprising similarities between high-entropy alloys and a class of complex steels which we refer here to as high-entropy steels.

The key idea behind high-entropy steels, as for conventional high-entropy alloys, lies in realizing massively alloyed solid solution phases by using five or more elements. From a thermodynamic standpoint the main emphasis, when aiming at designing such materials with respect to excellent strength, plastic yielding behavior, ductility, and toughness, should be placed on avoiding the occurrence of brittle intermetallic phases.

For this reason, systems based on a solid solution face-centered cubic matrix that is rich in Fe and Mn seemed to be a realistic starting point for further blending other components in. These two base elements are known to have excellent mutual solubility and reliable thermodynamic data are available. As a further obvious alloying component into such a solid solution matrix, we used interstitial C owing to its stabilizing effect on the face-centered cubic phase field. We further studied Al and Si as additional substitutional solid solution alloying components because these elements are known to help suppressing cementite formation and promoting the formation of improved oxide surface layers against corrosive attack.

This alloying concept could not be realized though by using equiatomic proportions of these five elements, as required by the classical high entropy alloying concept. The reason for this is twofold. Firstly, thermodynamic estimates strongly suggest that equiatomic alloying using these five elements would lead to a multi-phase structure rather than to a solid solution phase field. Secondly, from a thermodynamic standpoint, realizing a high configurational entropy contribution for stabilizing a single-phase field does actually not require using equiatomic component proportions, since the corresponding shape of the entropy curve as a function of chemical composition is very flat so that substantial deviations (see Table 1) from the equiatomic composition provide a similar configurational entropy as an equiatomic mix.

These considerations open novel pathways to the design of high-entropy steels on the basis of non-equiatomic matrix solid solutions with face-centered cubic crystal structure based for instance on the matrix elements Fe, Mn, Ni, C, N, and Co. Up to about 5–7 wt% Cr can also stabilize the austenitic phase field. Further alloying elements of interest would be Al and Si owing to their tendency to suppress the formation of carbides. It should be considered though that the latter components should be well controlled in their contribution, since they limit the face-centered cubic phase field. When highly alloyed by Mn, Ni, and C, high-entropy steels can also solve very high fractions of Al, i.e., up to 22 wt%.

The mechanical properties of the high entropy steels that we probed here are superior compared to those of many conventional austenitic Fe–Cr–Ni steels. We found values of the ultimate tensile strengths of up to 1000 MPa and tensile elongations reaching up to 100% in some cases. Also at cryogenic temperatures, tested down to −50 °C, the materials show outstanding ductility, i.e., up to 70% elongation to fracture in quasi-static tensile tests at −50 °C.

C as interstitial element in high-entropy steels was used —together with Mn—to tune the stacking fault energy levels. In this way, a sufficiently instable fcc matrix was compositionally designed for enabling deformation-induced athermal deformation mechanisms such as

twinning and martensite formation, i.e., TWIP and TRIP effects. The TRIP effect was documented in terms of the martensitic volume fractions formed during deformation and the associated excellent strain hardening behavior.

Many of the non-equiatomic Fe–Mn–Al–Si–C-based high-entropy steels presented in this paper have a VEC of 7–8 when only counting the substitutional elements. However, when additionally counting the electrons provided by interstitial C, the current alloys reach VECs above 8 suggesting a face-centered cubic phase.

Acknowledgments

The authors are grateful for funding of some of the work presented here through the Federal German Ministry for Research (BMBF) under the Grant number 03N3110D. Funding by the European Union is acknowledged, provided under the 7th Framework Programme through the ERC Advanced Grant SMARTMET and by the Directorate-General for Research and Innovation, Directorate G, Industrial Technologies, Unit G.5, Research Fund for Coal and Steel through the grant provided under the agreement RFSR-CT-2006-00027. Many discussions with the late Professor Georg Frommeyer are very gratefully acknowledged.

Received: April 9, 2015;
Published online: July 21, 2015

Keywords: high-entropy alloys; TWIP; TRIP; strain hardening; low-density steels

References

[1] A. J. B. Vincent, *BSc Part II Thesis*, University of Sussex, UK **1981**.
[2] P. Knight, *BSc Part II Thesis*, University of Oxford, Oxford, UK **1995**.
[3] B. Cantor, I. T. H. Chang, P. Knight, A. J. B. Vincent, *Mater. Sci. Eng. A* **2004**, *375*, 213.
[4] B. Cantor, *Ann. Chim. Sci. Mater.* **2007**, *32*, 245.
[5] K.-B. Kim, Y. Zhang, P. J. Warren, B. Cantor, *Philos. Mag.* **2003**, *83*, 2371.
[6] K.-B. Kim, P. J. Warren, B. Cantor, in *Metastable, Mechanically Alloyed and Nanocrystalline Materials 2002, Proc. of the 9th Int. Symp. on Metastable, Mechanically Alloyed and Nanocrystalline Materials ISMANAM-2002* (Eds: J.-H. Ahn, Y.-D. Hahn), Seoul, Korea, 8–12 September **2002**; Trans Tech Publications: Zurich -Durnten, Switzerland 2003, pp. 143–148.
[7] B. Cantor, *Entropy* **2014**, *16*, 4749.
[8] S. Ranganathan, *Curr. Sci.* **2003**, *85*, 1404.
[9] J. W. Yeh, S. K. Chen, S. J. Lin, J. Y. Gan, T. S. Chin, T. T. Shun, C. H. Tsau, S. Y. Chang, *Adv. Eng. Mater.* **2004**, *6*, 299.
[10] J. W. Yeh, *Ann. Chim. -Sci. Mater.* **2006**, *31*, 633.
[11] J. Antonaglia, X. Xie, Z. Tang, C.-W. Tsai, J. W. Qiao, Y. Zhang, M. O. Laktionova, E. D. Tabachnikova, R. Carroll, J. W. Yeh, O. N. Senkov, M. C. Gao, J. T. Uhl, P. K. Liaw, K. A. Dahmen, *JOM* **2014**, *66*, 2002.
[12] Y. Zhang, T. T. Zuo, Z. Tang, M. C. Gao, K. A. Dahmen, P. K. Liaw, Z. P. Lu, *Prog. Mater. Sci.* **2014**, *61*, 1.
[13] K. Y. Tsai, M. H. Tsai, J. W. Yeh, *Acta Mater.* **2013**, *61*, 4887.
[14] C. J. Tong, Y. L. Chen, S. K. Chen, J. W. Yeh, T. T. Shun, C. H. Tsau, S. J-Lin, S. Y. Chang, *Metal. Mater. Trans. A* **2005**, *36*, 881.
[15] C. J. Tong, M. R. Chen, S. K. Chen, J. W. Yeh, T. T. Shun, S. J-Lin, S. Y. Chang, *Metall. Mater. Trans.* **2005**, *36A*, 1263.
[16] J. W. Yeh, Y. L. Chen. S. J. Lin, S. K. Chen, *Mater. Sci. Forum* **2007**, *560*, 1.
[17] W. Hume-Rothery, *Acta Metall.* **1996**, *14*, 17.
[18] W. Hume-Rothery, *Acta Metall.* **1967**, *15*, 567.
[19] Y. Zhang, Y. Zhou, *Mater. Sci. Forum* **2007**, *561–565*, 1337.
[20] J. W. Yeh, S. K. Chen, J. Y. Gan, S. J. Lin, T. S. Chin, T. T. Shun, C. H. Tsau, S. Y. Chang, *Metall. Mater. Trans. A* **2004**, *35A*, 2533.
[21] X. Yang, Y. Zhang: *Mater. Chem. Phys.* **2012**, *132*, 233.
[22] S. Guo, Q. Hu, C. Ng, C. T. Liu, *Intermetallics* **2013**, *41*, 96.
[23] S. Guo, C. Ng, J. Lu, C. T. Liu, *J. Appl. Phys.* **2011**, *109*, 103505.
[24] U. Mizutani, Hume-Rothery Rules for Structurally Complex Alloy Phases, CRC Press, Boca Raton **2011**.
[25] B. Massalski, *Mater. Trans.* **2010**, *51*, 583.
[26] M. J. Yao, K. G. Pradeep, C. C. Tasan, D. Raabe, *Scr. Materialia* **2014**, *72–73*, 5.
[27] C. C. Tasan, Y. Deng, K. G. Pradeep, M. J. Yao, H. Springer, D. Raabe, *JOM* **2014**, *66*, 1993.
[28] F. Otto, Y. Yang, H. Bei, E. P. George, *Acta Mater.* **2013**, *61*, 2628.
[29] K. G. Pradeep, N. Wanderka, P. Choi, J. Banhart, B. S. Murty, D. Raabe, *Acta Mater.* **2013**, *61*, 4696.
[30] S. Singh, N. Wanderka, B. S. Murty, U. Glatzel, J. Banhart, *Acta Mater.* **2011**, *59*, 182.
[31] T. T. Shun, L. Y. Chang, M. H. Shiu, *Mater. Charact.* **2012**, *70*, 63.
[32] S. Singh, N. Wanderka, K. Kiefer, K. Siemensmeyer, J. Banhart, *Ultramicroscopy* **2011**, *111*, 619.
[33] B. Gludovatz, A. Hohenwarter, D. Catoor, E. H. Chang, E. P. George, R. O. Ritchie, *Science* **2014**, *345*, 1153.
[34] J. Y. He, W. H. Liu, H. Wang, Y. Wu, X. J. Liu, T. G. Nieh, Z. P. Lu, *Acta Mater.* **2014**, *62*, 105.
[35] O. Grässel, L. Krüger, G. Frommeyer, L. W. Meyer, *Int. J. Plast.* **2000**, *16*, 1391.
[36] S. Allain, J. P. Chateau, O. Bouaziz, *Mater. Sci. Eng. A* **2004**, *387*, 143.
[37] C. Scott, S. Allain, M. Faral, N. Guelton, *Rev. Metall.* **2006**, *103*, 293.

[38] J. D. Yoo, K-T Park, *Mater. Sci. Eng. A* **2008**, *496*, 417.
[39] J-K Kim, L. Chen, H-S Kim, S-K Kim, Y. Estrin, B. C. De Cooman, *Metall. Mater. Trans. A* **2009**, *40A*, 147.
[40] S. Curtze, V.-T. Kuokkala. *Acta Mater.* **2010**, *58*, 5129.
[41] H. Idrissi, K. Renard, D. Schryvers, P. J. Jacques. *Scr. Mater.* **2010**, *63*, 961.
[42] O. Bouaziz, S. Allain, C. P. Scott, P. Cugy, D. Barbier. *Curr. Opin. Solid State Mater Sci.* **2011**, *15*, 141.
[43] J-E Jin, Y-K Lee. *Acta Mater* **2012**, *60*, 1680.
[44] S. J. Lee, J. Kim, S. N. Kane, B. C. De Cooman, *Acta Mater.* **2011**, *59*, 6809.
[45] M. Koyama, T. Sawaguchi, T. Lee, C. S. Lee, K. Tsuzaki, *Mater. Sci. Eng. A* **2011**, *528* 7310.
[46] D. Barbier, V. Favier, B. Bolle, *Mater. Sci. Eng. A* **2012**, *540*, 212.
[47] O. Bouaziz, N. Guelton, *Mater. Sci. Eng. A* **2001**, *319*, 246.
[48] I. Karaman, H. Sehitoglu, A. J. Beaudoin, Y. I. Chumlyakov, H. J. Maier, C. N. Tome, *Acta Mater.* **2000**, *48*, 2031.
[49] S. Dancette, L. Delannay, K. Renard, M. A. Melchior, P. J. Jacques, *Acta Mater.* **2012**, *60*, 2135.
[50] S. Reeh, D. Music, D. T. Gebhardt, M. Kasprzak, T. Japel, S. Zaefferer, D. Raabe, S. Richter, A. Schwedt, J. Mayer, B. Wietbrock, G. Hirt, J. Schneider, *Acta Mater.* **2012**, *60*, 6025.
[51] S. Allain, J. P. Chateau, O. Bouaziz, *Steel Res.* **2002**, *73*, 299.
[52] A. Saeed-Akbari, L. Mosecker, A. Schwedt, W. Bleck, *Metall. Mater. Trans. A* **2012**, *43*, 1688.
[53] I. Gutierrez-Urrutia, D. Raabe, *Acta Mater.* **2011**, *59*, 6449.
[54] D. R. Steinmetz, T. Japel, B. Wietbrock, P. Eisenlohr, I. Gutierrez-Urrutia, A. Saeed-Akbari, T. Hickel, F. Roters, D. Raabe, *Acta Mater.* **2013** *61*, 494.
[55] I. Gutierrez-Urrutia, S. Zaefferer, D. Raabe, *Mater. Sci. Eng. A* **2010**, *527*, 3552.
[56] G. Frommeyer, U. Brüx, *Steel Res. Int.* **2006**, *77*, 627.
[57] M. Bausch, G. Frommeyer, H. Hofmann, E. Balichev, M. Soler, M. Didier, L. Samek, Research report, European Commission, Directorate-General for Research and Innovation, Directorate G, Industrial Technologies, Unit G.5, Research Fund for Coal and Steel, RFCS Publications, European Commission, Grant agreement RFSR-CT-**2006**-00027, ISBN: 978-92-79-22245-0
[58] O. Grässel, *Dissertation*, Max-Planck-Institut für Eisenforschung und TU Clausthal-Zellerfeld, Germany **2000**.
[59] O. Grässel, G. Frommeyer, C. Derder, H. Hofmann, *J. Phys. Fr.* **1997**, *7*, C5-383.
[60] U. Brüx, G. Frommeyer, O. Grässel, L.W. Meyer, L. Krüger, A. Weise, *Steel Res. Int.* **2002**, *73*, 294.
[61] G. Frommeyer, U. Brüx, P. Neumann, *ISIJ Int.* **2003**, *43*, 438.
[62] D. T. Pierce, J. A. Jimenez, J. Bentley, D. Raabe, C. Oskay, J. E. Wittig, *Acta Mater.* **2014**, *68*, 238.
[63] H. Springer, D. Raabe, *Acta Mater.* **2012**, *60*, 4950.
[64] I. Gutierrez-Urrutia, D. Raabe, *Acta Mater.* **2012**, *60*, 5791.
[65] I. Gutierrez-Urrutia, D. Raabe, *Scr. Mater.* **2013**, *68*, 343.
[66] I. Gutierrez-Urrutia, D. Raabe, *Mater. Sci. Technol.* **2014**, *30*, 1099.
[67] D. Raabe, H. Springer, I. Gutierrez-Urrutia, F. Roters, M. Bausch, J. B. Seol, M. Koyama, P. P. Choi, K. Tsuzaki, *JOM* **2014**, *66*, 1845.
[68] Y. Deng, C. C. Tasan, K. G. Pradeep, H. Springer, A. Kostka, D. Raabe, *Acta Mater.* **2015**, *94*, 124.
[69] V. Raynor, V. G. Rivilin, *Phase Equilibria in Iron Ternary Alloys*, Vol. 102, The Institute of Metals, London **1988**.
[70] O. Ishida, K. Ohtanik, N. Satoh, *ISIJ Int.* **1960**, *30*, 680.
[71] A. Forsberg, J. Ågren, *J. Phase Equilib.* **1993**, *14*, 354.
[72] J. E. Krzanowski, *Met. Trans.* **1985**, *16A*, 1689.
[73] U. Brüx, *Dissertation*, Max-Planck-Institut Düsseldorf and TU Clausthal-Zellerfeld, Germany **2007**.
[74] J.-B. Seol, D. Raabe, P. Choi, H.-S. Park, J.-H. Kwak, C.-G. Park, *Scr. Mater.* **2013**, *68*, 348.
[75] G. Frommeyer, *Private communication*, Max Planck Institut für Eisenforschung **2009**.
[76] J. P. Bressanell, A. Moskowitz, *Trans. ASM* **1966**, *59*, 223.
[77] G. L. Huang, D. K. Matlock, G. Krauss, *Metall. Trans. A* **1989**, *20A*, 1239.
[78] S. S. Hecker, M. G. Stout, K. P. Staudhammer, J. L. Smith, *Metall. Trans. A* **1982**, *13A*, 619.
[79] D. Raabe, *Metall. Mater. Trans. A* **1995**, *26*, 991.
[80] D. Raabe, *Mater. Sci. Technol.* **1995**, *11*, 461.
[81] D. Raabe, *Acta Mater.* **1997**, *45*, 1137.
[82] C. Herrera, D. Ponge, D. Raabe, *Acta Mater.* **2011**, *59*, 4653.
[83] C. Herrera, D. Ponge, D. Raabe, *Steel Res. Int.* **2008**, *79*, 482.
[84] M. Calcagnotto, D. Ponge, D. Raabe, *ISIJ Int.* **2012**, *52*, 874.
[85] M. Calcagnotto, D. Ponge, D. Raabe, *Metall. Mater. Trans. A* **2012**, *43*, 37.
[86] C. C. Tasan, M. Diehl, D. Yan, C. Zambaldi, P. Shanthraj, F. Roters, D. Raabe, *Acta Mater.* **2014**, *81*, 386.
[87] C. C. Tasan, J. P. N. Hoefnagels, M. Diehl, D. Yan, F. Roters, D. Raabe, *Int. J. Plast.* **2014**, *63*, 198.
[88] C. C. Tasan, M. Diehl, D. Yan, M. Bechtold, F. Roters, L. Schemmann, C. Zheng, N. Peranio, D. Ponge, M. Koyama, K. Tsuzaki, D. Raabe, *Annu. Rev. Mater. Res.* **2015**, *45*, 19.1.
[89] M. Calcagnotto, Y. Adachi, D. Ponge, D. Raabe, *Acta Mater.* **2011**, *59*, 658.
[90] M. Koyama, C. C. Tasan, E. Akiyama, K. Tsuzaki, D. Raabe, D. *Acta Mater.* **2014**, *70*, 174.
[91] M. Calcagnotto, D. Ponge, D. Raabe, *Mater. Sci. Eng. A* **2010**, *527*, 7832.

[92] M. Calcagnotto, D. Ponge, D. Raabe, *ISIJ Int.* **2008**, *48*, 1096.
[93] M.-M. Wang, C. C. Tasan, D. Ponge, A. Kostka, D. Raabe, *Acta Mater.* **2014**, *79*, 268.
[94] M.-M. Wang, C. C. Tasan, D. Ponge, A. -Ch. Dippel, D. Raabe, *Acta Mater.* **2015**, *85*, 216.
[95] O. Dmitrieva, D. Ponge, G. Inden, J. Millán, P. Choi, J. Sietsma, D. Raabe, *Acta Mater.* **2011**, *59*, 364.
[96] D. Raabe, S. Sandlöbes, J. Millán, D. Ponge, H. Assadi, M. Herbig, P. P. Choi, *Acta Mater.* **2013**, *61*, 6132.
[97] D. Raabe, D. Ponge, O. Dmitrieva, B. Sander, *Adv. Eng. Mater.* **2009**, *11*, 547.
[98] D. Raabe, D. Ponge, O. Dmitrieva, B. Sander, *Scr. Mater.* **2009**, *60*, 1141.
[99] L. Yuan, D. Ponge, J. Wittig, P. P. Choi, J. A. Jiménez, D. Raabe, *Acta Mater.* **2012**, *60*, 2790.